Endocytosis restricts synapse growth by attenuating Highwire/PHR1-dependent JNK signaling in a pathway parallel to the BMP signaling

Srikanth Pippadpally[1], Saumitra Dey Choudhury[1,3#], Anjali Bisht[1#], Manish Kumar Dwivedi[1#], Zeeshan Mushtaq[1#], Suneel Reddy-Alla[2], Vimlesh Kumar[1*]

[1] Department of Biological Sciences, Indian Institute of Science Education and Research (IISER) Bhopal, Academic Building 3, Bhauri, Bhopal-462 066, Madhya Pradesh, India.

[2] College of Community Science, Acharya N.G. Ranga Agricultural University, Guntur-522034, Andhra Pradesh, India

[3] Present Address: Centralized Core Research Facility (Microscopy) Convergence Block, All India Institute of Medical Sciences (AIIMS), Ansari Nagar, New Delhi- 110029, India

# Equal contribution

* Author for correspondence

Corresponding author: Phone - +91 755 2691405

Fax - +91 755 2692392

Email- vimlesh@iiserb.ac.in

Running title: JNK-dependent synaptic growth signaling in endocytic mutants

Keywords: AP2-complex; BMP pathway; JNK pathway; Highwire; Wallenda; Rab11; Synaptic growth signaling

Abstract

Endocytosis regulates the retrieval of synaptic membranes and the trafficking of growth signaling receptors. While *Drosophila* endocytic mutants show synaptic overgrowth at the neuromuscular junctions (NMJs), the signaling pathways by which endocytosis restricts synapse growth remain poorly understood. Here, we demonstrate that σ2-adaptin, one of the obligate subunits of the AP2 complex, facilitates the degradation and trafficking of E3-ubiquitin ligase Highwire (Hiw)/PHR1 and inhibits the c-Jun N-terminal kinase (JNK) signaling. This function of σ2-adaptin is independent of its Bone Morphogenetic Protein (BMP) signaling regulation. Loss of σ2-adaptin leads to Hiw accumulation and mislocalization in the neuronal cell body, leading to elevated MAP3K Wallenda levels. Stabilizing Hiw by expressing Rae1 or genetically blocking the JNK signaling suppresses the synaptic overgrowth defects observed in *σ2-adaptin* mutants. Remarkably, blocking BMP and JNK signaling pathways suppressed the synaptic overgrowth observed in the *σ2-adaptin* mutant to the wild-type levels. Finally, we show that loss of Rab11 but not Rab5 or Rab7 leads to accumulation/mislocalization of Hiw in the neuronal cell body akin to *σ2-adaptin* mutants. We propose a model in which endocytosis regulates Rab11-mediated Hiw trafficking and attenuates JNK signaling in a pathway parallel to the BMP signaling to restrict synaptic growth.

Introduction

Neuronal signaling mediated through endocytosis and endosomal trafficking are intimately linked and regulate synaptic development, growth, and plasticity. *Drosophila* endocytic mutants show altered bouton size and number, underscoring the importance of endocytosis in regulating synaptic growth (1-3). While the BMP pathway facilitates synaptic growth at the *Drosophila* NMJ, endocytosis restricts synaptic growth by internalizing and trafficking the BMP receptors. Genetically blocking the BMP signaling by mutating *wit* or *med* in endocytic mutants only partially restores the bouton size while significantly rescuing the bouton number, suggesting possible involvement of other signaling pathways in regulating synaptic growth.

Studies in *C. elegans* and *Drosophila* revealed that crosstalk between autophagy and MAP3K signaling is mediated through the E3-ubiquitin ligase Hiw/PHR1 (4,5). Autophagy induces synaptic growth by reducing Hiw levels, whereas Hiw negatively regulates synaptic growth by inhibiting the MAP3K Wallenda (Wnd), a key activator of the JNK pathway (4,5). Moreover, Hiw has also been implicated in the degradation of co-Smad Med, thus playing a pivotal role as a signaling hub in regulating the BMP and JNK signaling in neurons (6). Interestingly, while mutations in Medea only partially suppress the synaptic overgrowth, *wnd* mutants completely suppress the synaptic overgrowth observed in the *hiw* mutants (5,7). These genetic studies support the hypothesis that, similar to *hiw* mutants, endocytic mutants might regulate multiple signaling pathways that restrict synaptic growth.

Here, we show that: a) impaired endocytosis and endosomal trafficking result in the accumulation and mislocalization of Hiw in the neuronal cell body, thereby increasing Wnd level, which in turn activates the downstream JNK signaling, b) loss of Rab11 results in the accumulation of Hiw and Wnd in neurons akin to *σ2-adaptin* mutants, revealing a novel Rab11-

dependent trafficking of Hiw, and c) remarkably, inhibiting the BMP and JNK signaling restricts the synaptic overgrowth in *σ2-adaptin* mutant to the control levels.

Results

Loss of σ2-adaptin reduces autophagic degradation of Hiw and results in its accumulation in the neuronal cell body.

Studies in animal and cell culture models have shown a significant interdependency of endocytosis and autophagy in maintaining cellular homeostasis (8-10). Moreover, CME also plays a noncanonical role in the formation of autophagosomes and autophagy regulation in neurons (11-14). While autophagy plays a crucial role in regulating synaptic growth, its involvement in restricting synaptic overgrowth in the endocytic mutants remains poorly studied. To assess if autophagy was perturbed in the *Drosophila* endocytic mutants, we analyzed Atg8a levels (15,16) at the NMJ by expressing an Atg8a-GFP transgene in *σ2-adaptin* mutant neurons. We found a reduction in the levels of Atg8a-GFP in *σ2-adaptin* mutants, suggesting the perturbation of autophagy in these mutants (Figure S1A-D). Next, we analyzed autophagic flux in the *σ2-adaptin* mutants using GFP-mCherry-Atg8a, a well-established marker for assessing autophagic flux *in vivo* (Figure 1A) (17,18). Consistently, we found a reduction in the levels of both GFP and mCherry fluorescence (Figure 1B-D", F -H**)**. Analysis of another endocytic mutant *synj1* also showed similar results (Figure 1E-E", F-H), suggesting that while autophagic flux was not altered, autophagosome formation may be compromised in the endocytic mutants, leading to reduced autophagy.

In *Drosophila*, autophagy plays a crucial role in promoting synapse development by regulating the abundance of Hiw (19). As observed in AP2σ mutants, a reduction in autophagy would be expected to increase Hiw levels, thereby inhibiting synaptic growth by degrading Wallenda (5,6). However, contrary to this hypothesis, AP2σ mutants exhibit synaptic

overgrowth despite reduced autophagy, resembling *hiw* mutant phenotype (5,20). To investigate this discrepancy further, we analyzed Hiw fluorescence levels in larval ventral nerve cord (VNC) of endocytic mutants. Indeed, we found an increase in Hiw (GFP-Hiw) levels in the VNCs of *σ2-adaptin* mutants compared to the control (Figure 2C-C" and E-E", H-I). Surprisingly, high-resolution optical imaging revealed that the elevated GFP-Hiw was accumulated and possibly mislocalized in the neuronal cell body (Figure 2C-C" and E-E"). While the size of Hiw punctae was significantly large, the total number of punctae was reduced considerably in the *σ2-adaptin* mutant (Figure 2B-F" and J-K). Consistent with these findings, the knockdown of another AP2-complex subunit AP2α resulted in similar accumulations of GFP-Hiw in the neuronal cell body (Figure S2A-C). We found that expression of *UAS-GFP* in the *σ2-adaptin* mutant background did not cause any accumulation or increase in intensity, suggesting that the GFP-Hiw accumulations are not an artifact of overexpression (Figure 2B-F" and J-K). Autophagy mutants did not show an accumulation of Hiw-GFP despite an increase in its level (Figure S2D-G), suggesting a defect in Hiw trafficking in the endocytic mutants. Consistently, analysis of another endocytic mutant, *synj1* (21), also showed an accumulation of Hiw in the neuronal cell body (Figure 2G-K), similar to the *σ2-adaptin* mutants. Moreover, a reduction in synaptic Hiw levels in *σ2-adaptin* and *synj1* mutant NMJs further supports defective Hiw trafficking to synapses in these mutants, potentially due to their accumulation/mislocalization in the cell body (Figure S3). To further investigate the nature of GFP-Hiw accumulates, we examined their colocalization with Rabs and autophagy markers. Our analysis revealed that while Hiw accumulates did not colocalize with Rab5, Rab7 or Rab11 (Figure S4), they exhibited significant colocalization with the autophagic marker ref(2)P (p62 ortholog in *Drosophila*) (22,23) in *σ2-adaptin* mutants (Figure 2L-N). Together, these data strengthen our observation that compromised endocytosis leads to decreased autophagy-

dependent degradation of GFP-Hiw, resulting in increased Hiw levels and accumulation in the neuronal cell body.

Neuronal expression of Rae1 suppresses synaptic defects in *σ2-adaptin* mutants

To test if the accumulated Hiw is functional, we analyzed the effect of Hiw on synaptic overgrowth observed in *σ2-adaptin* mutants by neuronally expressing a functional GFP-Hiw transgene (24) (Figure 3A). We found that the expression of GFP-Hiw did not suppress the synaptic overgrowth of *σ2-adaptin* mutants (Figure 3B-F", H, and I). Interestingly, neuronal expression of Rae1, a protein that biochemically interacts with Hiw and stabilizes it (19,25), significantly suppressed the synaptic overgrowth phenotype in *σ2-adaptin* mutants, including bouton number and bouton size (Figure 3B-G", H and I). Since both the transgenes (Hiw and Rae1) are GFP-tagged, we could not analyze the direct effect of Rae1 on the Hiw-GFP accumulations. Together, these results indicate that accumulated Hiw was non-functional and could not degrade its target proteins, Wallenda (5) and possibly Medea (6), thus activating the downstream MAP3K and BMP signaling pathways.

Since Hiw targets Wnd for degradation (5), we assessed the Wnd levels in *σ2-adaptin* mutants. We found an elevated Wnd level in the *σ2-adaptin* mutants, restored to the control level by normalizing σ2-adaptin in neurons (Figure 3J-M" and N). Consistently, *synj1* mutants also showed accumulation of Hiw and elevated Wnd levels in the neuronal cell body (Figure S5). These data suggest that accumulated Hiw in the endocytic mutants was non-functional, leading to increased neuronal Wnd levels.

σ2-adaptin restricts c-Jun N-terminal Kinase (JNK) signaling in neurons

As reduced autophagy, accumulation of Hiw, and increased Wnd levels imply a potential increase in the JNK signaling, we directly examined the levels of JNK signaling in

σ2-adaptin mutants by expressing JNK reporter puckered (*puc*)-*lacZ* (26-28). We observed significantly elevated LacZ levels in the *σ2-adaptin* mutant VNCs, suggesting that JNK signaling was upregulated in the mutants (Figure 4A-C" and E). Similar results were obtained with the *synj1* mutants (Figure 4D-D" and E). A remarkable increase in *puc-lacZ* levels strongly suggests the activation of JNK signaling in the endocytic mutants. We hypothesized that if elevated JNK signaling plays an active role in inducing the synaptic overgrowth observed in the endocytic mutants, blocking the components of JNK signaling should rescue the synaptic defects. Since JNK (Basket (Bsk) in *Drosophila*) acts downstream of MAP3K Wnd, we expressed a dominant negative form of JNK/Bsk in *σ2-adaptin* mutant neurons. Consistent with our hypothesis, we observed a significant suppression of synaptic overgrowth phenotypes when a dominant negative form of JNK/Bsk was expressed in *σ2-adaptin* mutants (Figure 4F-J", N-O).

Multiple studies in *C. elegans*, *Drosophila*, and mammals have implicated endocytosis in attenuating BMP signaling-dependent synaptic growth (2,24,29-32). Since our data strongly suggest a functional requirement of Hiw-dependent JNK signaling in regulating the synaptic defects of endocytic mutants, we wondered about the relative contribution of both BMP and JNK signaling pathways in inducing synaptic growth. To analyze this, we expressed a dominant negative form of Fos (Bsk^{DN}), which functions downstream to JNK and mutated a copy of Tkv (tkv^{7}), one of the BMP receptors, in the *σ2-adaptin* mutant background. Remarkably, we found a suppression of both bouton number and bouton size observed in endocytic mutants to the wild-type level (Figure 4F-O). These findings indicate that a) the bouton number and bouton size are sensitive to both the BMP and JNK signaling, and b) remarkably, inhibiting BMP and JNK signaling pathways in endocytic mutants is necessary and sufficient to suppress the synaptic defects to the control levels.

Rab11 regulates Highwire trafficking in neurons

While our data show that elevated Hiw was accumulated in *σ2-adaptin* and *synj1* mutants, the autophagic mutants do not show such accumulation in the cell body despite increased Hiw levels (Figure S2D-G) (24). This suggests that in addition to the downregulated autophagy-dependent degradation of Hiw, endocytic mutants might have defective Hiw trafficking/localization in the neurons. Hence, to address whether Hiw trafficking depends on the endosomal system, we examined Hiw localization in animals neuronally expressing dominant negative forms of the endosomal trafficking proteins Rab5, Rab7 or Rab11. While expressing a dominant negative form of Rab5 ($Rab5^{S43N}$) or Rab7 ($Rab7^{T22N}$) did not affect Hiw trafficking, animals expressing a dominant negative Rab11 ($Rab11^{S25N}$) (33) in neurons showed Hiw accumulation in the neuronal cell body (Figure 5A-E). Consistent with these observations, Hiw accumulation and elevated Wallenda levels were observed in *Rab11* mutants (Figure 5F-M and Figure S6). Since Rab11 was found to be reduced in *σ2-adaptin* as well as *synj1* mutants (34), these results indicate that a) Rab11 independently functions in pathways regulating the autophagy-dependent degradation and trafficking of Hiw *in vivo*, and b) Hiw accumulates and possibly gets mislocalized due to compromised Rab11-dependent endosomal trafficking in the endocytic mutants.

Discussion

We identified a novel signaling pathway that involves Rab11-mediated Hiw trafficking to attenuate JNK signaling. We propose that BMP and JNK signaling functions in a parallel pathway to restrict NMJ growth. We provide multiple lines of evidence to support our major conclusion that deregulation of Highwire/PHR1-dependent JNK signaling underlies synaptic overgrowth phenotypes observed in the endocytic mutants.

Autophagy regulates protein turnover at the synapses, thereby regulating synaptic growth (19,35). Endocytosis is a crucial regulator of autophagy, influencing several pathways that determine the level of autophagy (10,36). For instance, the regulation of autophagy protein Atg9 trafficking by endosomes plays an essential role in autophagosome biogenesis (37,38). Importantly, the formation of autophagosomes utilizes endosomes as a significant source of membranes (10,39,40). This conclusion is corroborated by the observation that *σ2*-adaptin genetically interacts with the recycling endosomal protein Rab11, and its synaptic level was reduced in the *σ2-adaptin* mutants due to trafficking defects (34). Moreover, studies in cell culture and *in vitro* reconstitution studies have shown that Rab11 regulates the formation of recycling endosomes, which in turn are required for the formation of autophagosomes and the progression of autophagy (41-47). AP2 and Synj1 are involved in endocytosis-independent regulation of autophagy, suggesting the possibility of defective autophagy independent of endocytosis at synaptic terminals (48,49). Our data that blocking the JNK pathway alone can rescue the synaptic defects in the endocytic mutants suggests the possibility of an endocytosis/trafficking-dependent regulation of autophagy in synaptic development. Reduced autophagy increases the Hiw level but leads to its accumulation and possible mislocalization in the neuronal cell body in the endocytic mutants (Figure 2A). In contrast, while mutations in autophagy genes (for instance, *atg1*) lead to elevated Hiw levels, they do not accumulate in the neuronal cell body as they can rescue the synaptic phenotypes of autophagy mutants (19), further strengthening our conclusion that endocytic mutants have defective Hiw trafficking/localization in addition to reduced Hiw degradation. In *C. elegans*, RPM-1 has been shown to interact with the Rab guanine nucleotide exchange factor (GEF) GLO-4 and the Rab GTPase GLO-1 via late endosomes to regulate synaptic vesicular trafficking (50,51). This interaction further suggests that Rabs may help localize RPM-1/Hiw to specific neuronal compartments where it can affect synaptic development. Consistent with these data, our

observation that Hiw accumulates in the neuronal cell body of *Rab11* mutants akin to *σ2-adaptin* and s*ynj1* mutants further indicates the involvement of Rab11-dependent endosomal trafficking of Hiw in neurons (Figure 5).

A double mutant of *hiw* and *σ2-adaptin* resulted in early larval lethality, suggesting the possibility of their functioning in the same pathway. Our observation that stabilization of Hiw by expressing Rae1 rescues the synaptic defects in the *σ2-adaptin* mutants suggests that compromised ubiquitination activity of Hiw due to its accumulation or mislocalization resulted in increased Wnd/DLK1 levels in *σ2-adaptin* mutants. Wnd phosphorylates JNK, activating the transcription factor Fos to regulate synaptic growth (39). The analysis of JNK signaling reporter *puc-LacZ* in *σ2-adaptin* and *synj1* mutants further substantiated the direct activation of JNK signaling in the endocytic mutants (Figure 4).

Blocking the BMP pathway in endocytic mutants only partially suppressed the synaptic growth defects, suggesting the involvement of other signaling pathways in fine-tuning the different aspects of synaptic growth (6,34,52). Additionally, loss of Hiw results in synaptic overgrowth due to elevated JNK signaling, and blocking JNK signaling in the *hiw* mutants was sufficient to restore these synaptic defects (5,6,52). Thus, the BMP and JNK pathways cooperate to restrict synapse growth. Our finding that blocking JNK signaling in *σ2-adaptin* mutants by expressing a dominant negative form of JNK/Bsk or Fos suppressed the synaptic overgrowth phenotypes, including bouton number and bouton size, suggests that endocytosis parallelly regulates both BMP and JNK signaling to restrict the synaptic growth. Finally, our finding that blocking JNK signaling by expressing Fos^{DN} and blocking the BMP pathway by mutating a copy of Tkv in *σ2-adaptin* mutants attenuated the synaptic overgrowth and suppressed both the bouton number and bouton size to the wild-type levels suggested that indeed synaptic growth in endocytic mutants is sensitive to the levels of the both BMP and JNK signaling (52).

Seminal work by others has shown that post axonal injury, the downregulation of Hiw leads to an accumulation of Wnd, enhancing the JNK activation and facilitating axonal regeneration (53). Activated Wnd is transported retrogradely within the axons, initiating a signaling cascade essential for neuronal regeneration and survival (53,54). The interplay between these proteins is vital; while Wnd promotes growth and repair, excessive activation can lead to cell death (53,55,56). More recent data further implicates a role of Rab11 in coupling the localization of Wallenda to axons and protein turnover during stress response, suggesting a crucial role of Rab11-dependent trafficking and protein turnover (57). Consistent with these data, our findings implicate a direct role of endocytic proteins in the trafficking of Hiw and modulate their availability and activity, which may impact the neuronal response to axonal injury through Rab11-dependent trafficking mechanism (58).

Thus, a model emerges in which endocytosis attenuates synaptic growth, including bouton number and bouton size, by downregulating the JNK signaling (Figure 5N) through a pathway involving Rab11-dependent Hiw trafficking. Endocytosis facilitates BMP receptor internalization and trafficking (40-42), and Hiw regulates BMP (arguably by downregulating Med) and JNK (by downregulating Wnd/DLK1) pathways. Accumulation and defective Hiw trafficking (due to reduced Rab11 levels) combined with compromised BMP receptor internalization could underlie activation of the BMP and JNK pathway in the endocytic mutants, leading to synaptic overgrowth. This is the first study that uncovers the role of endocytosis and Rab11-mediated endosomal trafficking of Hiw in attenuating JNK-dependent NMJ growth in a pathway parallel to the BMP signaling.

Materials and Methods

Fly stocks

All the flies were grown and maintained at 25°C temperature in a standard cornmeal medium as described previously (59). w^{1118} was used as control unless otherwise mentioned.

Both males and females were used for experiments. The *σ2-adaptin* mutant alleles used were *AP2σ*^{ang7}, a hypomorphic allele generated through P-element mobilization of *Synd*^{EP877} located 2416 bp upstream of Syndapin ORF, and *AP2σ*^{KG0245}, a null allele of σ2-adaptin which has a P-element insertion in the third exon of σ2-adaptin ORF (59). The following fly stocks were used in the study: *AP2σ*^{KG02457} (BL13478), *atg1*$^{\Delta 3D}$ (60), *UAS-GFP-mCherry-Atg8a* (BL37749), *UAS-GFP-Atg8a* (BL52005), *UAS-GFP-Hiw* (BL51639), *UAS-AP2α RNAi* (GD15566), *GFP-Rae1* (25), *UAS-jnk*^{DN} (BL6409), *UAS-fos*^{DN} (BL7214), *synj1*^{1} (BL24883), *synj1*^{2} (BL24884), *Rab11*^{93Bi} and *Rab11*^{ex2} (61), *puc-lacZ* (62), *UAS-Rab5*^{S43N} (BL42703), *UAS-Rab7*$^{T22N\text{-}YFP}$ (BL9778), and *UAS-Rab11*$^{S25N\text{-}YFP}$ (BL23261).

Immunohistochemistry and imaging

Third instar wandering larvae were dissected in cold, calcium-free HL3 saline (pH 7.2) containing 70 mM NaCl, 5 mM KCl, 20 mM $MgCl_2$, 10 mM $NaHCO_3$, 5 mM Trehalose, 115 mM sucrose, and 5 mM HEPES and fixed in 4% paraformaldehyde for 30 min. Fillets were washed in PBS containing 0.15 % Triton X-100, blocked for one hour with 5% bovine serum albumin (BSA), and then incubated overnight with the primary antibody at 4°C. The primary antibodies used in the study are mouse anti-CSP (1:50) (DSHB), mouse anti-NC82 (1:100) (DSHB), rat anti-Elav (1:200) (DSHB), mouse anti-β-galactosidase (1:200) (DSHB), Rabbit anti-Wallenda (1:100, (5)) mouse anti-GFP (1:200, Roche, Basel, Switzerland), Rabbit anti-Ref(2)P (1:200; Abcam, Cambridge, UK), anti-Rab5 (1:500 (63) was a gift from Marino Zerial (Max Planck Institute, Germany), anti-Rab7 (1:500) and anti-Rab11 (1:500; (64,65)) antibodies were a gift from Tsubasa Tanaka (RIKEN Center for Developmental Biology, Japan). The secondary antibodies conjugated to Alexa Fluor 488, Alexa Fluor 568, and Alexa Flour 633 (Invitrogen, ThermoFisher Scientific, Waltham, MA, USA) were used at 1:800 dilution. The Alexa Fluor 488 or Rhodamine-conjugated anti-HRP (Jackson ImmunoResearch, Pennsylvania, USA) was used at 1:800 dilution.

For Wnd staining, larvae were dissected in ice-chilled 1X PBS and fixed on 3.7% formalin on ice for one hour. Larval fillets were blocked with 5% BSA for 1 hour, followed by overnight incubation with primary antibody anti-Wnd and anti-NC82 at 4°C (5). For GFP-mCherry-Atg8a staining, the larvae were dissected in cold, calcium-free HL3 saline and fixed for 15 minutes at room temperature in 4% PFA in PBS (pH 7.2). Larval fillets were mounted in VECTASHIELD (Vector Laboratories, California, USA), and images were captured with a laser scanning confocal microscope (FV3000, Olympus Corporation, Tokyo, Japan).

Quantifications and statistical analysis

NMJ 6/7 from the A2 hemisegment were captured to calculate the bouton number. All the CSP-positive boutons were counted manually in ImageJ/Fiji software (National Institutes of Health, Bethesda, USA). The number of boutons from each NMJ was normalized to the respective muscle area. For muscle area quantification, images from A2 hemisegment were captured using 20× objective, and the area was quantified using ImageJ/Fiji software. For bouton area quantification, all terminal type-II boutons from muscle 6/7 at A2 hemisegment were used, and the bouton area was calculated by drawing a free-hand sketch around CSP positive bouton using ImageJ. NMJs from muscle 4 were captured using a plan apochromat 60×, 1.42 NA objective for fluorescence intensity quantification. All the control and experimental fillets were processed similarly for each NMJ, and the fluorescence images were captured under the same settings for a particular experimental set. The average intensity was normalized to the control intensity.

To quantify the GFP-Hiw puncta number and size, z-projections of confocal images of third-instar larval VNCs were captured and stacked. Gaussian filter was applied to the images and thresholded. The analyzed particle function of ImageJ was used to quantify the puncta number and size. For Hiw intensity quantification, the individual VNC of all genotypes was captured with the same parameters, the region of interest (whole VNC) was manually selected,

and the integrated density was calculated using ImageJ and divided with the area of the ROI to obtain the average integrated density or the average fluorescence intensity. Similarly, individual neuronal cell bodies were marked using the GFP (*UAS-GFP*) positive area and added to the ROI manager. Using the ROI area, the intensity of GFP-Hiw and Elav were quantified for each neuronal cell body, averaged, and normalized. The NC82 positive area was marked as ROI, and the mean intensity was measured for Wnd and normalized with the corresponding NC82 intensity. To quantify the *puc-LacZ* expression, Elav-positive nuclei were marked in the z-stack images of the third instar larval VNCs, and the levels of β-galactosidase were quantified and normalized with the corresponding Elav levels (66).

A straight line of 8.5 µm was drawn across the neuronal cell body, and using the plot profile function of ImageJ, intensity line profiles were plotted. For multiple comparisons, one-way ANOVA followed by post hoc Tukey's or Student's t-test was used. All the n values and quantification values related to the statistical analysis are reported in Table S1. GraphPad Prism 8 (GraphPad Software Inc, California, USA) was used to plot all the graphs. Error bars in all the histograms represent SEM. *$p < 0.5$, **$p < 0.01$, ***$p < 0.001$, ns; not significant.

Acknowledgments

We thank Dr. Avital Rodal for sharing *rab11* mutants, Dr. Mohit Prasad for sharing the *puc-lacZ* fly lines, Dr. Guang-Chao Chen for the *atg1* mutant, and Dr. Chunlai Wu for the GFP-Rae1 fly lines. We also thank Dr. Aaron DiAntonio for sharing the Wallenda antibody, Dr. Tsubasa Tanaka for Rab7 and Rab11 antibodies, and Dr. Marino Zerial for Rab5 antibodies; the Bloomington *Drosophila* Stock Center (BDSC) for the fly stocks; Developmental Studies Hybridoma Bank (DSHB), the University of Iowa for monoclonal antibodies; and Dr. Varun Chaudhary for his helpful comments on this manuscript. We acknowledge the help from the central microscopy facility at IISER Bhopal. This work was supported by the Science and

Engineering Board (SERB) Project Grant CRG/2021/000599, the Government of India, and by intramural funds from the Indian Institute of Science Education and Research Bhopal to V.K.

Data availability

All data related to this manuscript are contained within the article.

Figure Legends

Figure 1: σ2-adaptin regulates autophagosome formation in neurons

(A) Cartoon representation showing trafficking of the GFP-mCherry-Atg8a during the autophagic process. In the early stages of autophagosome formation, both GFP and mCherry fluoresce, so the autophagosomes appear yellow due to the overlap of green and red fluorescence. During the later stages, the autophagosome fuses with the lysosome to form an autolysosome. The acidic environment of the lysosome quenches GFP but not mCherry, causing autolysosomes to appear red, indicating the completion of the autophagic process. (B-E") Confocal images of third instar larval VNC co-labeled for GFP (green) and mCherry (red) in control (*Elav-Gal4/+; UAS-GFP-mCherry-Atg8a/+*), *AP2σ* mutant (*Elav-Gal4/+; UAS-GFP-mCherry-Atg8a/+; AP2σ-^{KG02457}/AP2σ^{ang7}*), *AP2σ* rescue *(Elav-Gal4/+; UAS-GFP-mCherry-Atg8a/+; UAS-AP2σ, AP2σ-^{KG02457}/AP2σ^{ang7}*), and *synj1 mutant (Elav-Gal4/+; UAS-GFP-mCherry-Atg8a/+, synj1$^{1/2}$*). The scale bar in E" represents 40 µm. (F), (G) and (H) Histograms showing GFP-Atg8a, mCherry-Atg8a levels, and GFP to mCherry ratio in the neuronal cell body of indicated genotypes. At least 16 VNCs of each genotype were used for the quantification. All the corresponding values are shown in Table S1. The statistical analysis was done using one-way ANOVA followed by post-hoc Tukey's test. ***$p<0.001$, ns: not significant.

Figure 2: Loss of σ2-adaptin results in Hiw accumulation in the neuronal cell body

(A) Schematic representation of third instar larval VNC. The magnified view represents accumulation and possible mislocalization of the Hiw in the neuronal cell bodies of endocytic mutants. (B-G") Confocal images of the neuronal cell body in larval VNC co-labeled for GFP-Hiw (green) and Elav (magenta) in GFP control (*Elav-Gal4/+; UAS-GFP/+), GFP-Hiw* (*Elav-Gal4/+; UAS-GFP-Hiw/+*), *GFP; AP2σ* mutant (*Elav-Gal4/+; UAS-GFP/+; AP2σ-^{KG02457}/AP2σ^{ang7}*), *GFP-Hiw; AP2σ* mutant (*Elav-Gal4/+; UAS-GFP-Hiw/+; AP2σ-*

^{KG02457}/*AP2σ*^{ang7}), *AP2σ* rescue (*Elav-Gal4/+; UAS-GFP-hiw/+; UAS-AP2σ, AP2σ-*^{KG02457}/*AP2σ*^{ang7}), and *synj1* mutant (*Elav-Gal4/+; UAS-GFP-Hiw, synj1*$^{1/2}$). The scale bar in G" represents 5 µm. (H), (I), (J), and (K) Histograms showing the average intensity of GFP-Hiw in both the whole ventral nerve cord and individual neuronal cell bodies, number of GFP-Hiw puncta, and size of Hiw-GFP puncta in indicated genotypes. At least 10 VNCs of each genotype were used for the quantifications. (L-M") Confocal images of the neuronal cell body in larval VNC co-labeled for the GFP-Hiw (green) and Ref(2)P (magenta) in the indicated genotypes. The scale bar in M" represents 5 µm. (N) Intensity plot profile showing the intensity and colocalization of the GFP-Hiw (green) and Ref(2)P (magenta) in indicated genotypes. All the corresponding values are shown in Table S1. The statistical analysis was done using one-way ANOVA followed by post-hoc Tukey's test. ***p<0.001, ns: not significant.

Figure 3: Neuronal expression of *Rae1* suppresses the synaptic overgrowth in *σ*$_2$*-adaptin* mutants.

(A) Schematic representation of the third instar larval NMJ at muscle 6/7. The magnified view represents the part shown to represent the synaptic phenotypes. (B-G") Confocal images of muscle 6/7 NMJ immunolabeled for synaptic vesicle marker CSP (magenta) and neuronal membrane marker HRP (green) to show the synaptic growth phenotypes in control (*w*^{1118}), *GFP-Hiw* (*Elav-Gal4/+; UAS-GFP-Hiw/+*), *AP2σ* mutant (*AP2σ*^{KG02457}/*AP2σ*^{ang7}), *AP2σ* rescue (*Elav-Gal4/+; UAS-AP2σ, AP2σ*^{KG02457}/*AP2σ*^{ang7}), *GFP-Hiw; AP2σ* mutant (*Elav-Gal4/+; UAS-GFP-Hiw/+; AP2σ*^{KG02457}/*AP2σ*^{ang7}), and *GFP-Rae1; AP2σ* mutant (*Elav-Gal4/+; UAS-GFP-Rae1/+; AP2σ*^{ang7}/*AP2σ-*^{KG02457}). The scale bar in G" represents 10 µm. (H) and (I) Histograms showing the average bouton number and average bouton area at muscle 6/7 NMJ of A2 hemisegment for indicated genotypes. At least 9 NMJs of each genotype were used for quantifications. (J-M") Confocal images of third instar larval VNC co-labeled for Wnd (magenta) and NC82 (green) in indicated genotypes. The scale bar in M" represents 20 µm. (N)

Histogram showing the average fluorescence intensity of Wnd in indicated genotypes. At least 8 VNCs of each genotype were used for the quantification. All the corresponding values are shown in Table S1. The statistical analysis was done using one-way ANOVA followed by post-hoc Tukey's test. *p<0.1, ***p<0.001; ns, not significant.

Figure 4: σ2-adaptin restricts JNK signaling

(A-D") Confocal images of third instar larval VNC co-labelled for β-Gal (magenta) and Elav (green) in control (*puc-LacZ/+*), *puc-LacZ, AP2σ* mutant (*puc-LacZ, AP2σ-*^{KG02457}*/AP2σ*^{ang7}), *puc-LacZ, AP2σ* rescue (*Elav-Gal4/+; puc-LacZ, UAS-AP2σ, AP2σ-*^{KG02457}*/AP2σ*^{ang7}), and *synj1* mutant (*synj1*$^{1/2}$*; puc-LacZ/+*). The scale bar in D" represents 20 µm. (E) Histogram showing the β-Gal levels in the VNCs of indicated genotypes. At least 9 VNCs of each genotype were used for the quantification. (F-M") Confocal images of muscle 6/7 NMJ showing the synaptic growth in indicated genotypes immunolabeled for synaptic vesicle marker CSP (magenta) and neuronal membrane marker HRP (green). The scale bar in M" represents 10 µm. (N) and (O) Histograms showing the average bouton area and average bouton number from muscle 6-7 NMJ at A2 hemisegment for indicated genotypes. At least 9 NMJs of each genotype were used for the quantifications. All the corresponding values are shown in Table S1. The statistical analysis was done using one-way ANOVA followed by post-hoc Tukey's test. ***p<0.001; **p<0.01; ns, not significant.

Figure 5: Rab11 regulates Highwire trafficking in the neuronal cell body

(A-D) Confocal images of the neuronal cell body labeled for GFP-Hiw (green) in the indicated genotypes. The scale bar in D represents 5 µm. (E) Histogram showing the quantification of the number of GFP-Hiw puncta in the indicated genotypes. At least 8 VNCs of each genotype were used for the quantification. (F-G') Confocal images of the neuronal cell body co-labeled for GFP-Hiw (green) and Elav (magenta) in control (*Elav-Gal4/+; UAS-GFP-Hiw/+),* and *GFP-Hiw; Rab11* mutants (*Elav-Gal4/+; UAS-GFP-Hiw/+; Rab11*$^{ex2/93Bi}$). The scale bar in G'

represents 5 µm. (H and I) Histograms showing the number of GFP-Hiw puncta and the average size of the GFP-Hiw puncta in the neuronal cell body of indicated genotypes. At least 12 VNCs of each genotype were used for the quantification. (J-L") Confocal images of third instar larval VNC co-labeled for Wnd (magenta) and NC82 (green) in control (w^{1118}), *Rab11* ($Rab11^{ex2/93Bi}$), and *AP2σ* mutants ($AP2\sigma\text{-}^{KG02457}/AP2\sigma^{ang7}$). The scale bar in L" represents 10 µm. (M) Histograms showing the average fluorescence intensity of Wnd in indicated genotypes. At least 10 VNCs of each genotype were used for the quantification. All the corresponding values are shown in Table S1. The statistical analysis was done using one-way ANOVA followed by post-hoc Tukey's test (for E and L) or Student's t-test (for H and I). ***$p<0.001$, ns; not significant. (N) A proposed model for the regulation of synaptic growth in endocytic mutants. The model depicts a novel mechanism in which endocytosis regulates Rab11-positive recycling endosomes, which in turn modulates three possibly independent pathways to attenuate synaptic growth. First, Rab11 regulates endosomal trafficking of Hiw, and mislocalization/accumulation of Hiw leads to increased JNK signaling. Second, reduced Rab11 levels lead to reduced autophagosome formation, compromising autophagy and leading to elevated Hiw levels, which accumulate/mislocalize in the endocytic mutants. Third, Rab11 is involved in the trafficking of the BMP receptors, and reduced Rab11 levels lead to increased pMad levels in the endocytic mutants. Together, our model suggests that endocytosis restricts synaptic growth by restricting both BMP and JNK signaling in a parallel pathway mediated by Rab11-dependent endosomal trafficking.

References

1. Rodal, A. A., Motola-Barnes, R. N., and Littleton, J. T. (2008) Nervous wreck and Cdc42 cooperate to regulate endocytic actin assembly during synaptic growth. *J Neurosci* **28**, 8316-8325
2. O'Connor-Giles, K. M., Ho, L. L., and Ganetzky, B. (2008) Nervous wreck interacts with thickveins and the endocytic machinery to attenuate retrograde BMP signaling during synaptic growth. *Neuron* **58**, 507-518
3. Dickman, D. K., Lu, Z., Meinertzhagen, I. A., and Schwarz, T. L. (2006) Altered synaptic development and active zone spacing in endocytosis mutants. *Curr Biol* **16**, 591-598
4. Wu, C. L., Daniels, R. W., and DiAntonio, A. (2007) DFsn collaborates with Highwire to down-regulate the Wallenda/DLK kinase and restrain synaptic terminal growth. *Neural Dev* **2**
5. Collins, C. A., Wairkar, Y. P., Johnson, S. L., and DiAntonio, A. (2006) Highwire restrains synaptic growth by attenuating a MAP kinase signal. *Neuron* **51**, 57-69
6. McCabe, B. D., Hom, S., Aberle, H., Fetter, R. D., Marques, G., Haerry, T. E., Wan, H., O'Connor, M. B., Goodman, C. S., and Haghighi, A. P. (2004) Highwire regulates presynaptic BMP signaling essential for synaptic growth. *Neuron* **41**, 891-905
7. Collins, C. A., and DiAntonio, A. (2007) Synaptic development: insights from Drosophila. *Curr Opin Neurobiol* **17**, 35-42
8. Tooze, S. A., Abada, A., and Elazar, Z. (2014) Endocytosis and autophagy: exploitation or cooperation? *Cold Spring Harb Perspect Biol* **6**, a018358
9. Kakuta, S., Yamaguchi, J., Suzuki, C., Sasaki, M., Kazuno, S., and Uchiyama, Y. (2017) Small GTPase Rab1B is associated with ATG9A vesicles and regulates autophagosome formation. *Faseb J* **31**, 3757-3773
10. Birgisdottir, A. B., and Johansen, T. (2020) Autophagy and endocytosis - interconnections and interdependencies. *J Cell Sci* **133**
11. Kononenko, N. L., Classen, G. A., Kuijpers, M., Puchkov, D., Maritzen, T., Tempes, A., Malik, A. R., Skalecka, A., Bera, S., Jaworski, J., and Haucke, V. (2017) Retrograde transport of TrkB-containing autophagosomes via the adaptor AP-2 mediates neuronal complexity and prevents neurodegeneration. *Nat Commun* **8**, 14819
12. Tian, Y., Chang, J. C., Fan, E. Y., Flajolet, M., and Greengard, P. (2013) Adaptor complex AP2/PICALM, through interaction with LC3, targets Alzheimer's APP-CTF for terminal degradation via autophagy. *Proc Natl Acad Sci U S A* **110**, 17071-17076
13. Hernandez-Diaz, S., Ghimire, S., Sanchez-Mirasierra, I., Montecinos-Oliva, C., Swerts, J., Kuenen, S., Verstreken, P., and Soukup, S. F. (2022) Endophilin-B regulates autophagy during synapse development and neurodegeneration. *Neurobiol Dis* **163**
14. Soukup, S. F., Kuenen, S., Vanhauwaert, R., Manetsberger, J., Hernandez-Diaz, S., Swerts, J., Schoovaerts, N., Vilain, S., Gounko, N. V., Vints, K., Geens, A., De Strooper, B., and Verstreken, P. (2016) A LRRK2-Dependent EndophilinA Phosphoswitch Is Critical for Macroautophagy at Presynaptic Terminals. *Neuron* **92**, 829-844
15. Mauvezin, C., Ayala, C., Braden, C. R., Kim, J., and Neufeld, T. P. (2014) Assays to monitor autophagy in Drosophila. *Methods* **68**, 134-139
16. Low, P., Varga, A., Pircs, K., Nagy, P., Szatmári, Z., Sass, M., and Juhász, G. (2013) Impaired proteasomal degradation enhances autophagy via hypoxia signaling in Drosophila. *Bmc Cell Biol* **14**
17. Chakravorty, A., Sheeba, V., and Manjithaya, R. (2024) Drosophila melanogaster Neuromuscular Junction as a Model to Study Synaptopathies and Neuronal Autophagy. in *Neuroprotection: Method and Protocols* (Ray, S. K. ed.), Springer US, New York, NY. pp 97-120
18. Brazill, J. M., Zhu, Y., Li, C., and Zhai, R. G. (2018) Quantitative Cell Biology of Neurodegeneration in

Through Unbiased Analysis of Fluorescently Tagged Proteins Using ImageJ. *Jove-J Vis Exp*
19. Shen, W., and Ganetzky, B. (2009) Autophagy promotes synapse development in. *J Cell Biol* **187**, 71-79
20. Wan, H. I., DiAntonio, A., Fetter, R. D., Bergstrom, K., Strauss, R., and Goodman, C. S. (2000) Highwire regulates synaptic growth in Drosophila. *Neuron* **26**, 313-329
21. Verstreken, P., Koh, T. W., Schulze, K. L., Zhai, R. G., Hiesinger, P. R., Zhou, Y., Mehta, S. Q., Cao, Y., Roos, J., and Bellen, H. J. (2003) Synaptojanin is recruited by Endophilin to promote synaptic vesicle uncoating. *Neuron* **40**, 733-748
22. Nezis, I. P., Simonsen, A., Sagona, A. P., Finley, K., Gaumer, S., Contamine, D., Rusten, T. E., Stenmark, H., and Brech, A. (2008) Ref(2)P, the Drosophila melanogaster homologue of mammalian p62, is required for the formation of protein aggregates in adult brain. *J Cell Biol* **180**, 1065-1071
23. Bartlett, B. J., Isakson, P., Lewerenz, J., Sanchez, H., Kotzebue, R. W., Cumming, R. C., Harris, G. L., Nezis, I. P., Schubert, D. R., Simonsen, A., and Finley, K. D. (2011) p62, Ref(2)P and ubiquitinated proteins are conserved markers of neuronal aging, aggregate formation and progressive autophagic defects. *Autophagy* **7**, 572-583
24. Wu, C. L., Wairkar, Y. P., Collins, C. A., and DiAntonio, A. (2005) function at the

neuromuscular junction:: Spatial, structural, and temporal requirements. *J Neurosci* **25**, 9557-9566
25. Tian, X., Li, J., Valakh, V., DiAntonio, A., and Wu, C. (2011) Drosophila Rae1 controls the abundance of the ubiquitin ligase Highwire in post-mitotic neurons. *Nat Neurosci* **14**, 1267-1275
26. Zhu, S. J., Chen, R., Soba, P., and Jan, Y. N. (2019) JNK signaling coordinates with ecdysone signaling to promote pruning of

sensory neuron dendrites. *Development* **146**
27. Agnes, F., Suzanne, M., and Noselli, S. (1999) The Drosophila JNK pathway controls the morphogenesis of imaginal discs during metamorphosis. *Development* **126**, 5453-5462
28. Martín-Blanco, E., Gampel, A., Ring, J., Virdee, K., Kirov, N., Tolkovsky, A. M., and Martinez-Arias, A. (1998) puckered encodes a phosphatase that mediates a feedback loop regulating JNK activity during dorsal closure in Drosophila. *Gene Dev* **12**, 557-570
29. Gleason, R. J., Vora, M., Li, Y., Kane, N. S., Liao, K., and Padgett, R. W. (2017) SMA-10 regulates BMP receptor trafficking. *Plos One* **12**
30. Ehrlich, M. (2016) Endocytosis and trafficking of BMP receptors: Regulatory mechanisms for fine-tuning the signaling response in different cellular contexts. *Cytokine Growth F R* **27**, 35-42
31. Jacomin, A. C., Bescond, A., Soleilhac, E., Gallet, B., Schoehn, G., Fauvarque, M. O., and Taillebourg, E. (2015) The Deubiquitinating Enzyme UBPY Is Required for Lysosomal Biogenesis and Productive Autophagy in. *Plos One* **10**
32. Gleason, R. J., Akintobi, A. M., Grant, B. D., and Padgett, R. W. (2014) BMP signaling requires retromer-dependent recycling of the type I receptor. *P Natl Acad Sci USA* **111**, 2578-2583
33. Bellen, H. J., Levis, R. W., Liao, G., He, Y., Carlson, J. W., Tsang, G., Evans-Holm, M., Hiesinger, P. R., Schulze, K. L., Rubin, G. M., Hoskins, R. A., and Spradling, A. C. (2004) The BDGP gene disruption project: single transposon insertions associated with 40% of Drosophila genes. *Genetics* **167**, 761-781
34. Choudhury, S. D., Dwivedi, M. K., Pippadpally, S., Patnaik, A., Mishra, S., Padinjat, R., and Kumar, V. (2022) AP2 Regulates Thickveins Trafficking to Attenuate NMJ Growth Signaling in Drosophila. *eNeuro* **9**
35. Hoffmann-Conaway, S., Brockmann, M. M., Schneider, K., Annamneedi, A., Rahman, K. A., Bruns, C., Textoris-Taube, K., Trimbuch, T., Smalla, K. H., Rosenmund, C., Gundelfinger, E. D., Garner, C. C., and Montenegro-Venegas, C. (2020) Parkin contributes to synaptic vesicle autophagy in Bassoon-deficient mice. *Elife* **9**

36. Andres-Alonso, M., Kreutz, M. R., and Karpova, A. (2021) Autophagy and the endolysosomal system in presynaptic function. *Cell Mol Life Sci* **78**, 2621-2639
37. Holzer, E., Martens, S., and Tulli, S. (2024) The Role of ATG9 Vesicles in Autophagosome Biogenesis. *J Mol Biol* **436**
38. Yang, S. S., Park, D., Manning, L., Hill, S. E., Cao, M., Xuan, Z., Gonzalez, I., Dong, Y. M., Clark, B., Shao, L., Okeke, I., Almoril-Porras, A., Bai, J. H., De Camilli, P., and Colón-Ramos, D. A. (2022) Presynaptic autophagy is coupled to the synaptic vesicle cycle via ATG-9. *Neuron* **110**, 824-+
39. Puri, C., Renna, M., Bento, C. F., Moreau, K., and Rubinsztein, D. C. (2013) Diverse Autophagosome Membrane Sources Coalesce in Recycling Endosomes. *Cell* **154**, 1285-1299
40. Ravikumar, B., Moreau, K., Jahreiss, L., Puri, C., and Rubinsztein, D. C. (2010) Plasma membrane contributes to the formation of pre-autophagosomal structures (vol 12, pg 747, 2010). *Nat Cell Biol* **12**, 1021-1021
41. Zulkefli, K. L., Houghton, F. J., Gosavi, P., and Gleeson, P. A. (2019) A role for Rab11 in the homeostasis of the endosome-lysosomal pathway. *Exp Cell Res* **380**, 55-68
42. Bartz, R., Benzing, C., and Ullrich, O. (2003) Reconstitution of vesicular transport to Rab11-positive recycling endosomes in vitro. *Biochem Bioph Res Co* **312**, 663-669
43. Green, E. G., Ramm, E., Riley, N. M., Spiro, D. J., Goldenring, J. R., and WesslingResnick, M. (1997) Rab11 is associated with transferrin-containing recycling compartments in K562 cells. *Biochem Bioph Res Co* **239**, 612-616
44. Ullrich, O., Reinsch, S., Urbé, S., Zerial, M., and Parton, R. G. (1996) Rab11 regulates recycling through the pericentriolar recycling endosome. *J Cell Biol* **135**, 913-924
45. Longatti, A., and Tooze, S. A. (2012) Recycling endosomes contribute to autophagosome formation. *Autophagy* **8**, 1682-1683
46. Longatti, A., Lamb, C. A., Razi, M., Yoshimura, S., Barr, F. A., and Tooze, S. A. (2012) TBC1D14 regulates autophagosome formation via Rab11-and ULK1-positive recycling endosomes. *J Cell Biol* **197**, 659-675
47. Wilcke, M., Johannes, L., Galli, T., Mayau, V., Goud, B., and Salamero, J. (2000) Rab11 regulates the compartmentalization of early endosomes required for efficient transport from early endosomes to the trans-golgi network. *J Cell Biol* **151**, 1207-1220
48. Vanhauwaert, R., Kuenen, S., Masius, R., Bademosi, A., Manetsberger, J., Schoovaerts, N., Bounti, L., Gontcharenko, S., Swerts, J., Vilain, S., Picillo, M., Barone, P., Munshi, S. T., de Vrij, F. M., Kushner, S. A., Gounko, N. V., Mandemakers, W., Bonifati, V., Meunier, F. A., Soukup, S. F., and Verstreken, P. (2017) The SAC1 domain in synaptojanin is required for autophagosome maturation at presynaptic terminals. *EMBO J* **36**, 1392-1411
49. Bera, S., Camblor-Perujo, S., Barca, E. C., Negrete-Hurtado, A., Racho, J., De Bruyckere, E., Wittich, C., Ellrich, N., Martins, S., Adjaye, J., and Kononenko, N. L. (2020) AP-2 reduces amyloidogenesis by promoting BACE1 trafficking and degradation in neurons. *Embo Rep* **21**
50. Opperman, K. J., and Grill, B. (2014) RPM-1 is localized to distinct subcellular compartments and regulates axon length in GABAergic motor neurons. *Neural Dev* **9**
51. Grill, B., Bienvenut, W. V., Brown, H. M., Ackley, B. D., Quadroni, M., and Jin, Y. S. (2007) RPM-1 regulates axon termination and synaptogenesis through the Rab GEF GLO-4 and the Rab GTPase GLO-1. *Neuron* **55**, 587-601
52. Collins, C. A., and DiAntonio, A. (2007) Synaptic development:: insights from. *Current Opinion in Neurobiology* **17**, 35-42
53. Xiong, X., Wang, X., Ewanek, R., Bhat, P., Diantonio, A., and Collins, C. A. (2010) Protein turnover of the Wallenda/DLK kinase regulates a retrograde response to axonal injury. *J Cell Biol* **191**, 211-223
54. Hayne, M., and DiAntonio, A. (2022) Protein phosphatase 2A restrains DLK signaling to promote proper Drosophila synaptic development and mammalian cortical neuron survival. *Neurobiol Dis* **163**, 105586

55. Goel, P., and Dickman, D. (2018) Distinct homeostatic modulations stabilize reduced postsynaptic receptivity in response to presynaptic DLK signaling. *Nat Commun* **9**, 1856
56. Valakh, V., Walker, L. J., Skeath, J. B., and DiAntonio, A. (2013) Loss of the spectraplakin short stop activates the DLK injury response pathway in Drosophila. *J Neurosci* **33**, 17863-17873
57. Kim, S., Quagraine, Y., Singh, M., and Kim, J. H. (2024) Rab11 suppresses neuronal stress signaling by localizing Dual leucine zipper kinase to axon terminals for protein turnover. *bioRxiv*
58. Li, T., Shi, W., Ho, M. S., and Zhang, Y. Q. (2024) A Pvr–AP-1–Mmp1 signaling pathway is activated in astrocytes upon traumatic brain injury. eLife Sciences Publications, Ltd
59. Choudhury, S. D., Mushtaq, Z., Reddy-Alla, S., Balakrishnan, S. S., Thakur, R. S., Krishnan, K. S., Raghu, P., Ramaswami, M., and Kumar, V. (2016) sigma2-Adaptin Facilitates Basal Synaptic Transmission and Is Required for Regenerating Endo-Exo Cycling Pool Under High-Frequency Nerve Stimulation in Drosophila. *Genetics* **203**, 369-385
60. Scott, R. C., Schuldiner, O., and Neufeld, T. P. (2004) Role and regulation of starvation-induced autophagy in the

fat body. *Dev Cell* **7**, 167-178
61. Khodosh, R., Augsburger, A., Schwarz, T. L., and Garrity, P. A. (2006) Bchs, a BEACH domain protein, antagonizes Rab11 in synapse morphogenesis and other developmental events. *Development* **133**, 4655-4665
62. Ring, J. M., and Martinez Arias, A. (1993) puckered, a gene involved in position-specific cell differentiation in the dorsal epidermis of the Drosophila larva. *Dev Suppl*, 251-259
63. Mottola, G., Classen, A. K., Gonzalez-Gaitan, M., Eaton, S., and Zerial, M. (2010) A novel function for the Rab5 effector Rabenosyn-5 in planar cell polarity. *Development* **137**, 2353-2364
64. West, R. J. H., Lu, Y. B., Marie, B., Gao, F. B., and Sweeney, S. T. (2015) Rab8, POSH, and TAK1 regulate synaptic growth in a

model of frontotemporal dementia. *J Cell Biol* **208**, 931-947
65. Tanaka, T., and Nakamura, A. (2008) The endocytic pathway acts downstream of Oskar in Drosophila germ plasm assembly. *Development* **135**, 1107-1117
66. Xiong, X., Wang, X., Ewanek, R., Bhat, P., DiAntonio, A., and Collins, C. A. (2010) Protein turnover of the Wallenda/DLK kinase regulates a retrograde response to axonal injury. *J Cell Biol* **191**, 211-223

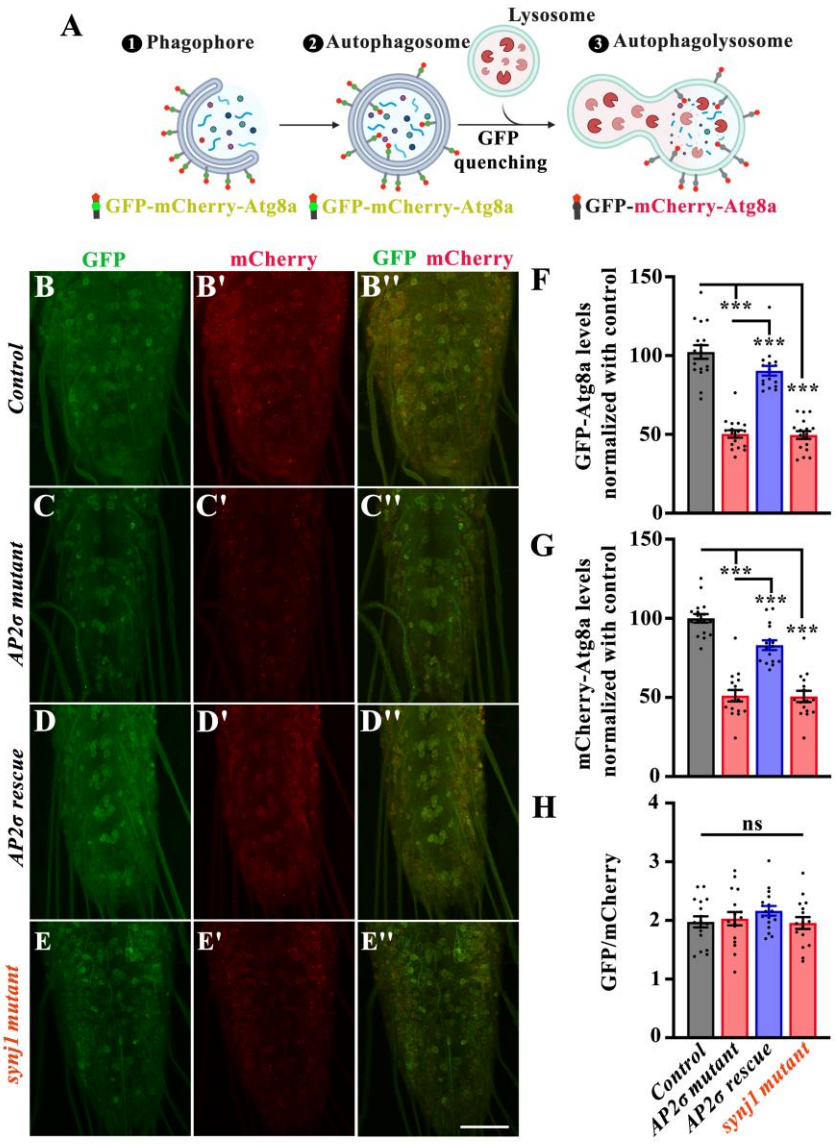
A
Lysosome
❶ Phagophore
❷ Autophagosome
❸ Autophagolysosome
GFP quenching
GFP-mCherry-Atg8a
GFP-mCherry-Atg8a
GFP-mCherry-Atg8a
GFP
mCherry
GFP mCherry
Control
AP2σ mutant
AP2σ rescue
synj1 mutant
B
B'
B''
C
C'
C''
D
D'
D''
E
E'
E''
F
GFP-Atg8a levels normalized with control
150
100
50
0
***
***
***
G
mCherry-Atg8a levels normalized with control
150
100
50
0
***
***
***
H
GFP/mCherry
4
3
2
1
0
ns
Control
AP2σ mutant
AP2σ rescue
synj1 mutant

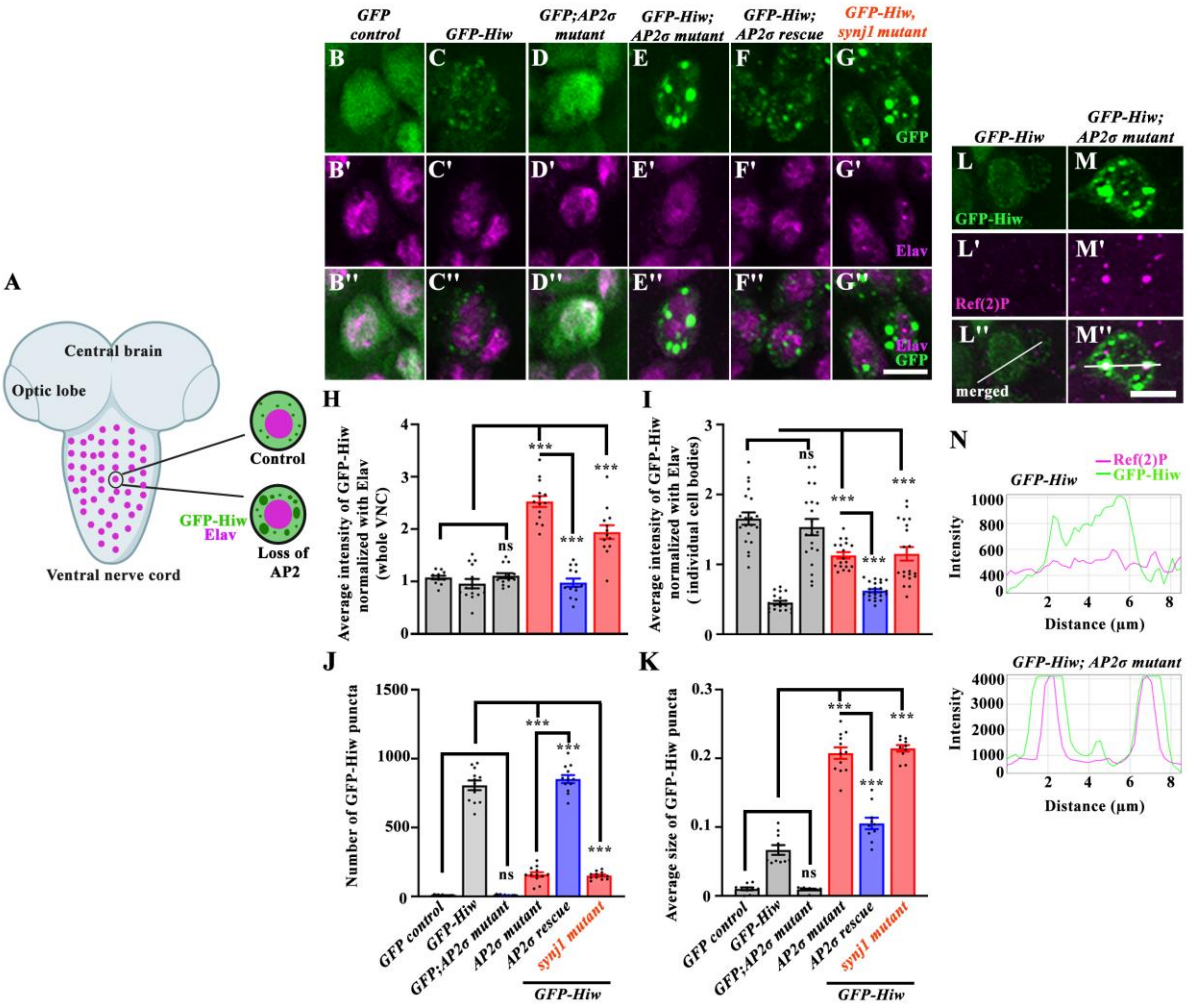
A
Central brain
Optic lobe
Ventral nerve cord
Control
GFP-Hiw
Elav
Loss of AP2
GFP control
GFP-Hiw
GFP;AP2σ mutant
GFP-Hiw; AP2σ mutant
GFP-Hiw; AP2σ rescue
GFP-Hiw, synj1 mutant
GFP
Elav
Elav GFP
GFP-Hiw
Ref(2)P
merged
H
Average intensity of GFP-Hiw normalized with Elav (whole VNC)
I
Average intensity of GFP-Hiw normalized with Elav (individual cell bodies)
J
Number of GFP-Hiw puncta
K
Average size of GFP-Hiw puncta
ns
***
GFP control
GFP-Hiw
GFP;AP2σ mutant
AP2σ mutant
AP2σ rescue
synj1 mutant
GFP-Hiw
N
Ref(2)P
GFP-Hiw
Intensity
Distance (μm)
GFP-Hiw; AP2σ mutant

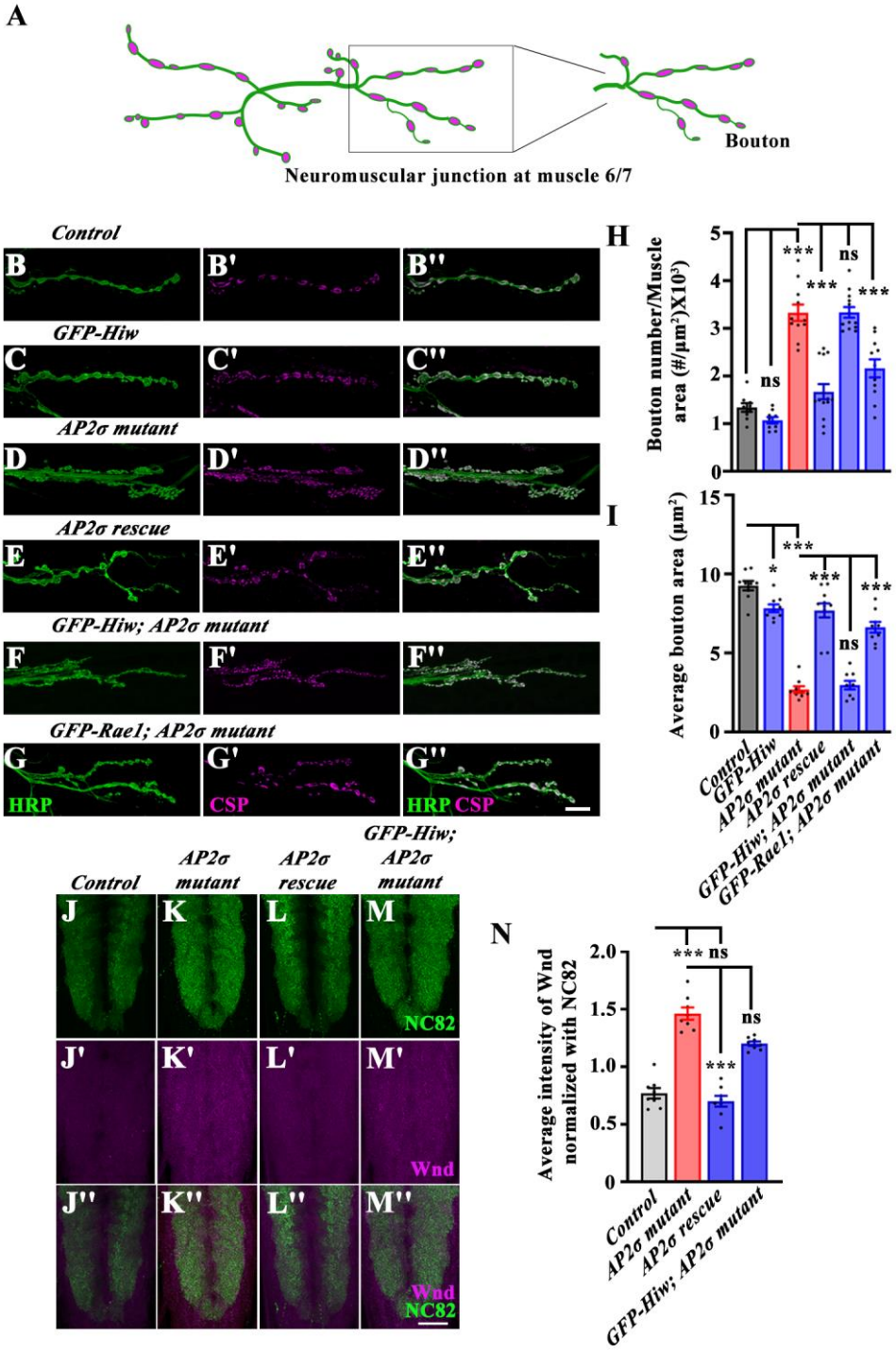
A
Bouton
Neuromuscular junction at muscle 6/7
Control
GFP-Hiw
AP2σ mutant
AP2σ rescue
GFP-Hiw; AP2σ mutant
GFP-Rae1; AP2σ mutant
B
B'
B''
C
C'
C''
D
D'
D''
E
E'
E''
F
F'
F''
G
G'
G''
HRP
CSP
HRP CSP
H
Bouton number/Muscle area (#/μm²)X10³)
I
Average bouton area (μm²)
Control
GFP-Hiw
AP2σ mutant
AP2σ rescue
GFP-Hiw; AP2σ mutant
GFP-Rae1; AP2σ mutant
J
K
L
M
NC82
J'
K'
L'
M'
Wnd
J''
K''
L''
M''
Wnd
NC82
N
Average intensity of Wnd normalized with NC82
Control
AP2σ mutant
AP2σ rescue
GFP-Hiw; AP2σ mutant

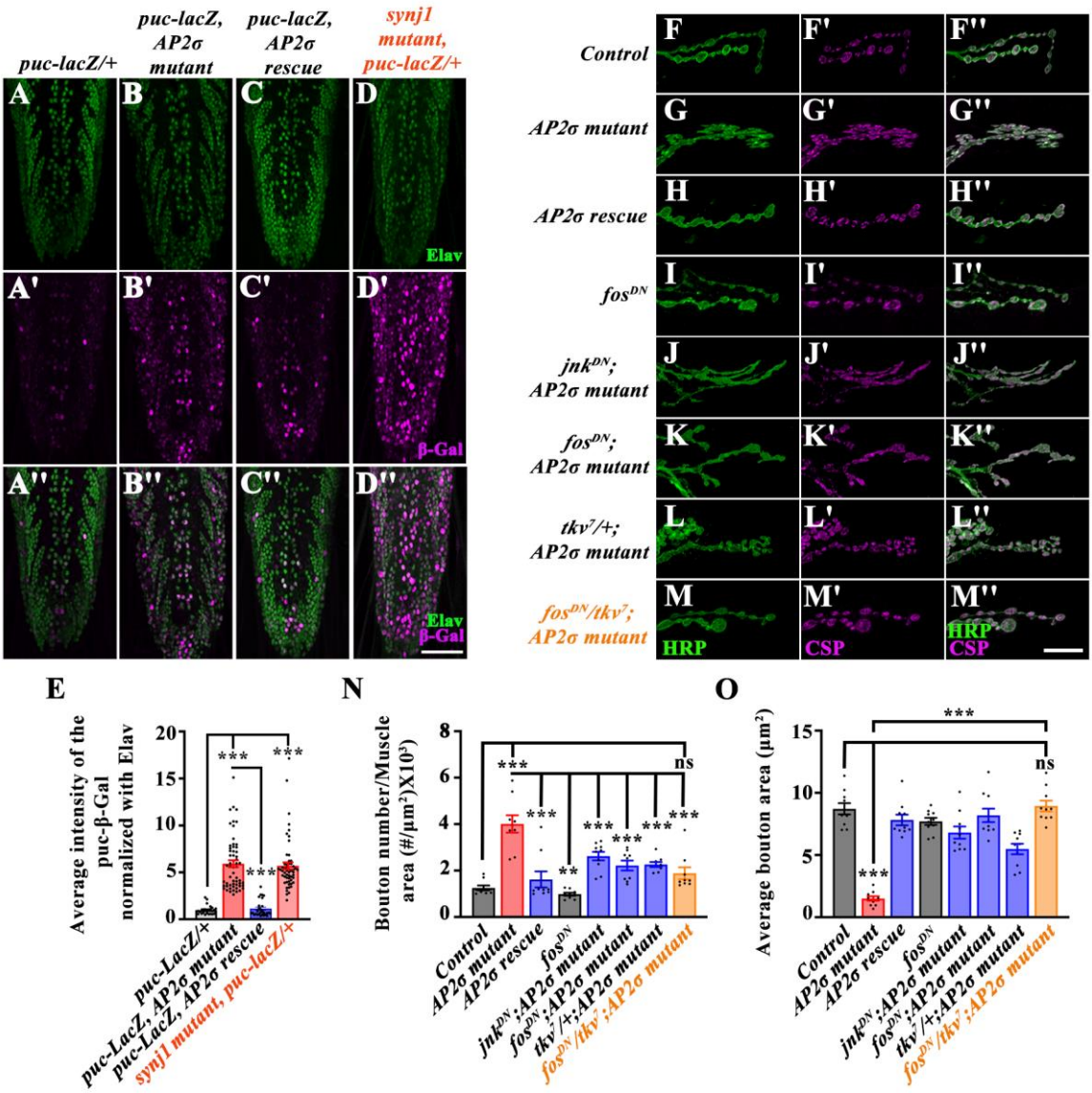
puc-lacZ/+
puc-lacZ, AP2σ mutant
puc-lacZ, AP2σ rescue
synj1 mutant, puc-lacZ/+
A
B
C
D
Elav
A'
B'
C'
D'
β-Gal
A''
B''
C''
D''
Elav
β-Gal
Control
AP2σ mutant
AP2σ rescue
fosDN
jnkDN; AP2σ mutant
fosDN; AP2σ mutant
tkv7/+; AP2σ mutant
fosDN/tkv7; AP2σ mutant
F
F'
F''
G
G'
G''
H
H'
H''
I
I'
I''
J
J'
J''
K
K'
K''
L
L'
L''
M
M'
M''
HRP
CSP
HRP
CSP
E
Average intensity of the puc-β-Gal normalized with Elav
N
Bouton number/Muscle area (#/μm²)X10³
O
Average bouton area (μm²)
***
**
ns

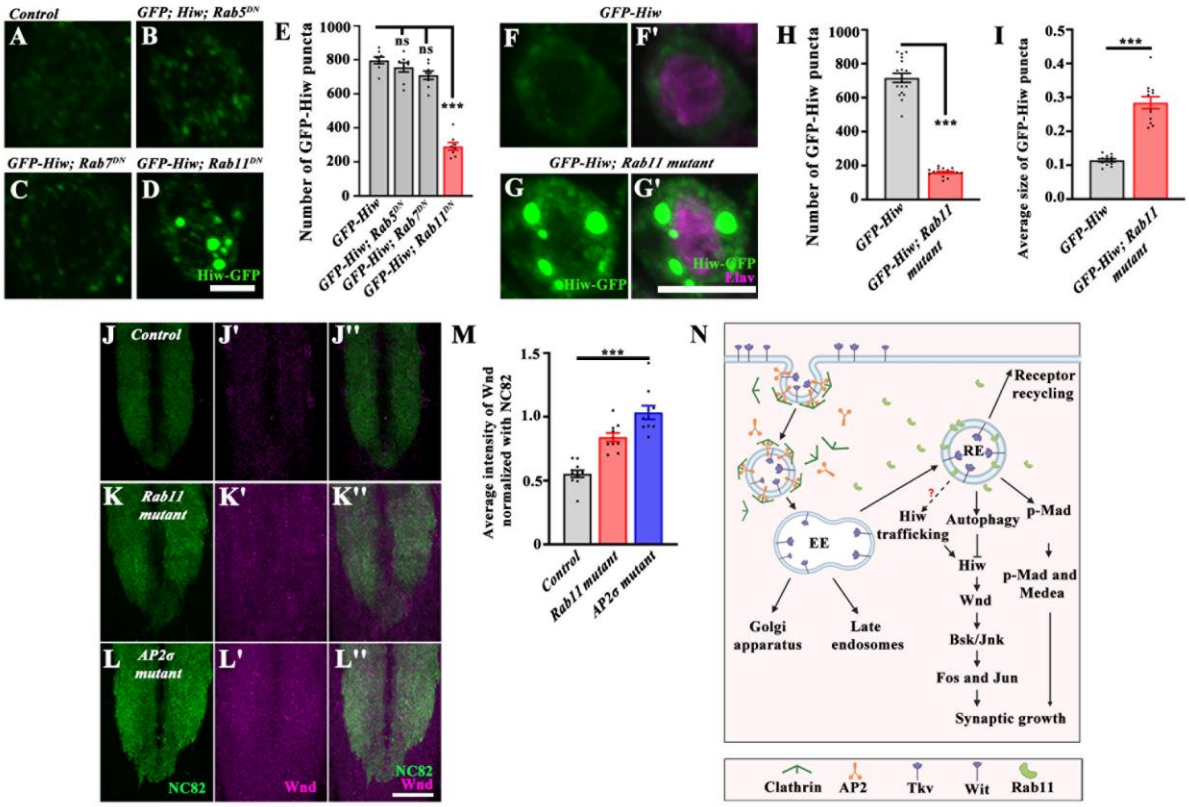
Control
GFP; Hiw; Rab5DN
GFP-Hiw; Rab7DN
GFP-Hiw; Rab11DN
Hiw-GFP
Number of GFP-Hiw puncta
ns
ns
***
GFP-Hiw
GFP-Hiw; Rab5DN
GFP-Hiw; Rab7DN
GFP-Hiw; Rab11DN
GFP-Hiw
GFP-Hiw; Rab11 mutant
Hiw-GFP
Hiw-GFP
Elav
Number of GFP-Hiw puncta
Average size of GFP-Hiw puncta
GFP-Hiw; Rab11 mutant
Control
Rab11 mutant
AP2σ mutant
NC82
Wnd
NC82
Wnd
Average intensity of Wnd normalized with NC82
Control
Rab11 mutant
AP2σ mutant
Receptor recycling
RE
EE
Hiw trafficking
Autophagy
p-Mad
Hiw
Wnd
Bsk/Jnk
Fos and Jun
Synaptic growth
p-Mad and Medea
Golgi apparatus
Late endosomes
Clathrin
AP2
Tkv
Wit
Rab11